Neuroprotective role of gap junctions in a neuron astrocyte network model

G. Huguet, A. Joglekar, L. Matamba Messi, R. Buckalew, S. Wong, D. Terman

Running title: Neuroprotective role of gap junctions

Key words: Computational model, spreading depolarization, K^+ buffering

Abstract

A detailed biophysical model for a neuron/astrocyte network is developed in order to explore mechanisms responsible for the initiation and propagation of cortical spreading depolarizations and the role of astrocytes in maintaining ion homeostasis, thereby preventing these pathological waves. Simulations of the model illustrate how properties of spreading depolarizations, such as wave-speed and duration of depolarization, depend on several factors, including the neuron and astrocyte Na^+-K^+ ATPase pump strengths. In particular, we consider the neuroprotective role of astrocyte gap junction coupling. The model demonstrates that a syncytium of electrically coupled astrocytes can maintain a physiological membrane potential in the presence of an elevated extracellular K^+ concentration and efficiently distribute the excess K^+ across the syncytium. This provides an effective neuroprotective mechanism for delaying or preventing the initiation of spreading depolarizations.

Introduction

Both cortical spreading depression and spreading depolarizations correspond to slowly propagating waves of rapid, near-complete depolarization of brain cells [1–6]. Cortical spreading depression typically arises in normal tissue, as in migraine, while spreading depolarizations typically arise in metabolically compromised tissue, as in ischemia [1, 4, 7, 8]. Both are characterized by a disruption of transmembrane ionic gradients, the collapse of ion homeostasis, cell swelling and elevated extracellular K^+ levels.

Cell damage and death during ischemia result from reduced oxygen and glucose supply to brain cells [1, 3, 6, 9]. This decreases mitochondrial ATP production, leading to failure of the Na^+-K^+ ATPase pump, which, in turn, leads to the rapid accumulation of Na^+ and chloride ions inside the cell, elevated extracellular K^+ ions, cell swelling and, ultimately, recurrent spreading depolarizations in both neurons and astrocytes. Depolarization of excitatory neurons stimulates an excessive release of the neurotransmitter glutamate leading to excitotoxicity.

Astrocytes play a central role in brain homeostasis and, therefore, may critically affect the development and outcome of both cortical spreading depression and spreading depolarizations [10–14]. Several studies have demonstrated that astrocytes are required for the recovery of pathologically elevated extracellular K^+ levels, which initiate spreading depolarizations, and in reducing high extracellular glutamate [15, 16].

In this paper, we develop a computational model for a neuron/astrocyte network in order to explore mechanisms responsible for the initiation and propagation of spreading depolarizations and the role of astrocytes in maintaining ion homeostasis, thereby preventing these waves. While there have been numerous previous papers that have developed detailed models to address various issues related to the spreading depression [17–32], the model presented here is the first to incorporate a detailed biophysical model for the astrocytes. This allows us to explore more fully the role of specific astrocyte processes in preventing pathological wave propagation.

In particular, we consider the role of gap junction connections between astrocytes. The neuroprotective role of gap junctions during diseased states has been under considerable debate [33, 34]. Numerous experimental results suggest that depending on the severity of injury, gap junction communication may either be beneficial following injury or amplify ischemic damage. In a recently published paper, we demonstrated both experimentally and with a computational model that a syncytium of electrically coupled astrocytes can maintain a physiological membrane potential in the presence of an elevated extracellular increase in K^+ concentration and efficiently distribute the excess K^+ across the syncytium [35]. Here we extend this model to a neuron/astrocyte network and demonstrate that a syncytium of electrically coupled astrocytes provides an effective mechanism for delaying or preventing spreading depression and depolarizations. However, gap junctions may also play a role in amplifying these signals, once they are initiated.

Methods: Model Equations

A schema of our model is shown in Figure 1. The model consists of a one dimensional array of astrocyte-neuron pairs sharing an extracellular space. The neuron and astrocyte models include equations for membrane potential, ionic currents, and ionic fluxes, as well as balance equations for $Na^+$and K^+concentrations inside the cells and in the shared extracellular space. Neurons are not coupled, and communicate only through ionic diffusion in the extracellular space, while astrocytes may be connected to other astrocytes by gap junctions which carry ionic currents and fluxes.

Neurons. Each neuron is modeled as a single compartment using the Hodgkin-Huxley formalism [36]. This model is similar to that in previous modeling studies of spreading depression [17–32]; however, our neuron model is minimal in the sense that it includes only those ionic currents required to generate the dynamics considered in this paper.

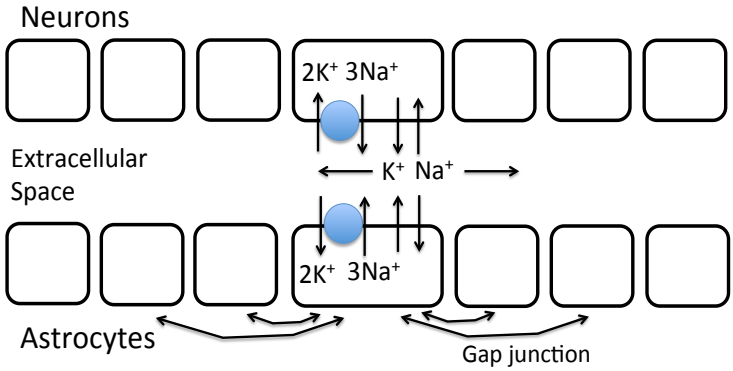

Figure 1: Schema of model. There is a one dimensional array of neurons, astrocytes and compartments corresponding to extracellular space. Each neuron and astrocyte has K^+ and Na^+ channels and a Na^+-K^+ ATPase pump, represented as a blue circle. K^+ and Na^+ ions diffuse in the extracellular space, as well as through gap junctions among the astrocytes.

The neuron's membrane potential V_N satisfies an equation of the form

$$C_m \frac{dV_N}{dt} = -I_{Na} - I_{NaP} - I_K - I_L - I_{P,N}$$

where I_{Na}, I_{NaP}, I_K and I_L correspond to fast Na^+, persistent Na^+, K^+ and leak currents,

respectively. These are given by

$$\begin{aligned} I_{Na} &= g_{Na}\, m_\infty^3(V_N)\, (1-n)\, (V_N - E_{Na,N}) \\ I_{NaP} &= g_{NaP}\, m_{p\infty}(V_N)\, h_p\, (V_N - E_{Na,N}) \\ I_K &= g_K\, n^4\, (V_N - E_{K,N}) \\ I_L &= g_L\, (V_N - E_L). \end{aligned}$$

Here, h_p and n are dynamic variables satisfying equations of the form

$$\frac{dX}{dt} = \phi_X \frac{X_\infty(V_N) - X}{\theta_X(V_N)},$$

where $X = h_p$ and n.

The asymptotic functions are of the form

$$X_\infty(V) = \frac{1}{1 + \exp\left(-(V - V_X)/\tau_X\right)},$$

where $V_m = -34, \tau_m = 5, V_n = -55, \tau_n = 14, V_{m_p} = -40, \tau_{m_p} = 6,$ and $V_{h_p} = -48$ and $\tau_{h_p} = 6$. Moreover,

$$\theta_n(V) = 0.05 + \frac{0.27}{1 + \exp((V+40)/12)} \quad \text{and} \quad \theta_{h_p}(V) = \frac{10000}{\cosh\left((V+49)/12\right)}.$$

The reversal potentials are given by

$$E_{K,N} = \frac{RT}{F} \ln\left(\frac{[\mathrm{K}^+]_e}{[\mathrm{K}^+]_{i,N}}\right) \quad \text{and} \quad E_{Na,N} = \frac{RT}{F} \ln\left(\frac{[\mathrm{Na}^+]_e}{[\mathrm{Na}^+]_{i,N}}\right)$$

where R, T and F are the gas constant, temperature and Faraday's constant, respectively.

As in [30], the Na^+-K^+ATPase pump current is given by

$$I_{P,N} = \rho_N \left(\frac{[\mathrm{K}^+]_e}{K_{K,N} + [\mathrm{K}^+]_e}\right)^2 \left(\frac{[\mathrm{Na}^+]_{i,N}}{K_{Na,N} + [\mathrm{Na}^+]_{i,N}}\right)^3,$$

where ρ_N represents the maximal pump current.

Parameters corresponding to the neurons are given in Table 1.

Astrocytes. The astrocytes are modeled as in [35]. As with neurons, each astrocyte is modeled as a single compartment using the Hodgkin-Huxley formalism; however, following [35], the currents are modeled using the Goldman-Hodgkin-Katz equations. We use the GHK formulation to account for strongly rectifying currents at nonphysiological ionic concentrations that occur in spreading depression / depolarization.

Table 1: Neuron parameters.

Notation	Value	Unit	Description
R	8.31	J/mol K	Ideal gas constant
F	96485	C/mol	Faraday's constant
T	310	K	Absolute temperature
C_m	1.00	μF/cm^2	Membrane capacitance per unit area
ϕ_n	0.80	ms^{-1}	Maximum rate of activation of potassium channels
ϕ_h	0.05	ms^{-1}	Maximum rate of activation of sodium channels
g_{Na}	3.0	mS/cm^2	Maximum fast sodium current conductance
g_{NaP}	0.4	mS/cm^2	Maximum persistent sodium current conductance
g_K	5.0	mS/cm^2	Maximum delayed rectifier potassium conductance
g_L	0.3	mS/cm^2	Non specific leak current conductance
E_L	-70.0	mV	Leak current reversal potential
ρ_N	Parameter	μA/cm^2	Maximum neuron Na^+-K^+-ATPase pump current
S_N	922	μm^2	Neuron total membrane surface area
Ω_N	2160	μm^3	Neuron total volume
α_0	0.10		Volume fraction between a neuron and astrocyte and the extracellular space
$K_{K,N}$	2	mM	Half activation $[K^+]$ concentration for the neural Na^+-K^+ATPase
$K_{Na,N}$	7.7	mM	Half activation $[Na^+]$ concentration for the neural Na^+-K^+ATPase

Each astrocyte's membrane potential, V_A, satisfies an equation of the form

$$C_m^A \frac{dV_A}{dt} = -I_{Na,A} - I_{K,A} - I_{P,A} - I_{gap},$$

where the K^+ and fast Na^+ currents are now given by

$$\begin{aligned} I_{K,A} &= P_K F \phi \left(\frac{[K^+]_e e^{-\phi} - [K^+]_{i,A}}{e^{-\phi} - 1} \right) \\ I_{Na,A} &= P_{Na} F \phi \left(\frac{[Na^+]_e e^{-\phi} - [Na^+]_{i,A}}{e^{-\phi} - 1} \right), \end{aligned}$$

respectively. Here P_K and P_{Na} are the K^+ and Na^+ permeability constants, $[K^+]_{i,A}$ and $[Na^+]_{i,A}$ are the K^+ and Na^+ concentrations in the astrocyte's cytosol, and $\phi = V_A F/RT$. Similar to the neurons, the Na^+-K^+ ATPase pump current is modeled as:

$$I_{P,A} = \rho_A \left(\frac{[K^+]_e}{K_{K,A} + [K^+]_e} \right)^2 \left(\frac{[Na^+]_{i,A}}{K_{Na,A} + [Na^+]_{i,A}} \right)^3 .$$

Currents due to the gap junctions are modeled using the Goldman-Hodgkin-Katz constant field equation with the potential difference across the gap junction as the driving force. Suppose there is a gap junction between astrocytes j and k. Denote the membrane potentials and intracellular ion concentrations of these cells as $(V_A^j, [K^+]_{i,A}^j, [Na^+]_{i,A}^j)$ and $(V_A^k, [K^+]_{i,A}^k, [Na^+]_{i,A}^k)$, respectively. Let

$$\phi^{jk} = \frac{F}{RT} \left(V_A^j - V_A^k \right)$$

and

$$\begin{aligned} I_{K,gap}^{jk} &= P_{K,gap} F \phi^{jk} \left(\frac{[K^+]_{i,A}^k e^{-\phi^{jk}} - [K^+]_{i,A}^j}{e^{-\phi^{jk}} - 1} \right), \\ I_{Na,gap}^{jk} &= P_{Na,gap} F \phi^{jk} \left(\frac{[Na^+]_{i,A}^k e^{-\phi^{jk}} - [Na^+]_{i,A}^j}{e^{-\phi^{jk}} - 1} \right). \end{aligned}$$

Here, $P_{K,gap}$ and $P_{Na,gap}$ are the K^+ and Na^+ gap junction permeabilities, averaged over the entire cell membrane. As in [35], we assume that

$$P_{K,gap} = \sigma_{gap}\, P_K \qquad \text{and} \qquad P_{Na,gap} = 0.8 \cdot P_{K,gap}$$

for a constant σ_{gap}. Then, for the cell j we set

$$I_{K,gap}^j = \sum I_{K,gap}^{jk} \qquad \text{and} \qquad I_{Na,gap}^j = \sum I_{Na,gap}^{jk}$$

where the sums are over all indices k for which there is a gap junction between cells j and k. Finally, let

$$I_{gap}^j = I_{K,gap}^j + I_{Na,gap}^j.$$

Parameters corresponding to the astrocytes are given in Table 2.

Ion concentrations. The neurons' intracellular K^+ and Na^+ concentrations satisfy the equations:

$$\begin{aligned} \frac{d[K^+]_{i,N}}{dt} &= -\frac{S_N}{F\,\Omega_N} \left(I_K - 2I_{P,N} \right) \\ \frac{d[Na^+]_{i,N}}{dt} &= -\frac{S_N}{F\,\Omega_N} \left(I_{Na} + I_{NaP} + 3I_{P,N} \right), \end{aligned}$$

Table 2: Astrocyte parameters.

Notation	Value	Unit	Description
P_K	4.8 10^{-6}	cm/s	Membrane K^+ permeability coefficient
P_{Na}	1.5 10^{-8}	cm/s	Membrane Na^+ permeability coefficient
S_A	1600	μm^2	Astrocyte total membrane surface area
Ω_A	2000	μm^3	Astrocyte total volume
C_m^a	1.00	$\mu F/cm^2$	Membrane capacitance per unit area
ρ_A	Parameter	$\mu A/cm^2$	Maximum astrocyte Na^+-K^+-ATPase pump current
σ_{gap}	Parameter	unitless	Measure of gap junction strength
$K_{K,A}$	2	mM	Half activation $[K^+]$ concentration for the astrocytic Na^+-K^+ATPase
$K_{Na,A}$	7.7	mM	Half activation $[Na^+]$ concentration for the astrocytic Na^+-K^+ATPase

where S_N is the neuron's surface area and Ω_N is the volume of the neuron's cytoplasm. Similarly, the astrocyte's intracellular K^+ and Na^+ concentrations satisfy the equations:

$$\begin{aligned}\frac{d[\mathrm{K}^+]_{i,A}}{dt} &= -\frac{S_A}{F\,\Omega_A}\left(I_{K,A} - 2I_{P,A} - I_{K,gap}\right)\\ \frac{d[\mathrm{Na}^+]_{i,A}}{dt} &= -\frac{S_A}{F\,\Omega_A}\left(I_{Na,A} + 3I_{P,A} - I_{Na,gap}\right),\end{aligned}$$

where S_A is the astrocyte's surface area and Ω_A is the volume of the astrocyte's cytoplasm.

We assume that K^+ and Na^+ ions diffuse in the extracellular space. In the continuum limit, where the number of cells become unbounded, these extracellular ionic concentrations satisfy equations of the form

$$\begin{aligned}\frac{\partial[\mathrm{K}^+]_e}{\partial t} &= \overline{D}_K\frac{\partial^2[\mathrm{K}^+]_e}{\partial x^2} + \frac{S_N}{F\,\Omega_E}\left(I_K - 2I_{P,N}\right) + \frac{S_A}{F\,\Omega_E}\left(I_{K,A} - 2I_{P,A}\right)\\ \frac{\partial[\mathrm{Na}^+]_e}{\partial t} &= \overline{D}_{Na}\frac{\partial^2[\mathrm{Na}^+]_e}{\partial x^2} + \frac{S_N}{F\,\Omega_E}\left(I_{Na} + I_{NaP} + 3I_{P,N}\right)\\ &\quad + \frac{S_A}{F\,\Omega_E}\left(I_{Na,A} + 3I_{P,A}\right),\end{aligned}$$

where Ω_E is the volume of the extracellular space, assumed to be a fixed fraction of the total volume, given by $\Omega_E = \alpha_0(\Omega_N + \Omega_A)$.

We simulated injecting K^+ into the extracellular space of a neuron/astrocyte pair by adding a positive constant, ϵ, to the right hand side of the equation for $[K^+]_e$ corresponding to those cells.

We use Dirichlet boundary conditions to simulate healthy tissue at the boundaries, with $[K^+]_{e,bdry} = 3.5$ mM and $[Na^+]_{e,bdry} = 138$ mM. The numerics correspond to an 'ischemic insult' to the network's center.

Numerics. Network simulations were performed in XPPAUT [37] and MATLAB (Mathworks, Inc.). The model was integrated variously using XPPAUT, MATLAB's ode15s, and an implicit 4^{th} order Runge-Kutta method implemented in C.

Results

Initiation of Waves. We start the system at rest and then simulate the injection of K^+ at a constant rate into the extracellular space of some subset neuron/astrocyte pairs. As the extracellular K^+ concentration, $[K^+]_e$, increases, the neuron's resting potential also increases. There is a $[K^+]_e$ threshold beyond which the corresponding neurons quickly depolarize, extruding additional K^+, and this initiates a wave of spreading depolarization. The time it takes for $[K^+]_e$ to reach this threshold depends on both the rate at which $[K^+]_e$ is increased and the rate at which $[K^+]_e$ is sequestered by the astrocytes and neurons. This latter rate is determined by several factors including the strength of the ATPase pumps, the maximal conductance of K^+ channels and the strength of astrocytic gap junction coupling, as well as diffusion of K^+ in the extracellular medium.

Clearly, strengthening the influx of K^+ across the membrane by ATPase pumps and K^+ channels leads to greater uptake of extracellular K^+ and, therefore, a longer delay before a wave is initiated. It is less clear why adding gap junctions between astrocytes results in a longer delay or even failure to initiate a wave. This will be discussed later.

Simulations. Some representative solutions of the model are shown in Figure 2. For each simulation, we consider a network of 50 neuron/astrocyte pairs. We start the network at rest and then simulate the injection of K^+ to the extracellular space of the middle cells 24, 25, 26, and 27 at a rate of 5 mM/sec. For these simulations, we vary the following parameters: i) ρ_N and ρ_A, the maximal strength of the neuron and astrocyte Na^+-K^+ ATPase pump currents, respectively; ii) σ_{gap}, a measure of the maximal conductance of a gap junction that is formally defined in the Methods section; and N, where each astrocyte has gap junction connections to its N closest neighbors on each side (for a total of $2N$ connections). If an astrocyte near one of the two edges of the network has fewer than N neighbors on one of its sides, then we assume that the astrocyte shares a gap junction with only those other astrocytes on that side.

Increasing pump strengths lengthens the delay and shortens recovery time, while adding gap junctions causes a larger delay and increases the speed propagation, visible as the slope of the wavefront. For example, Figure 2C shows that if $\rho_N = \rho_A = 5$, $\sigma_{gap} = 0.1$ and $N = 3$,

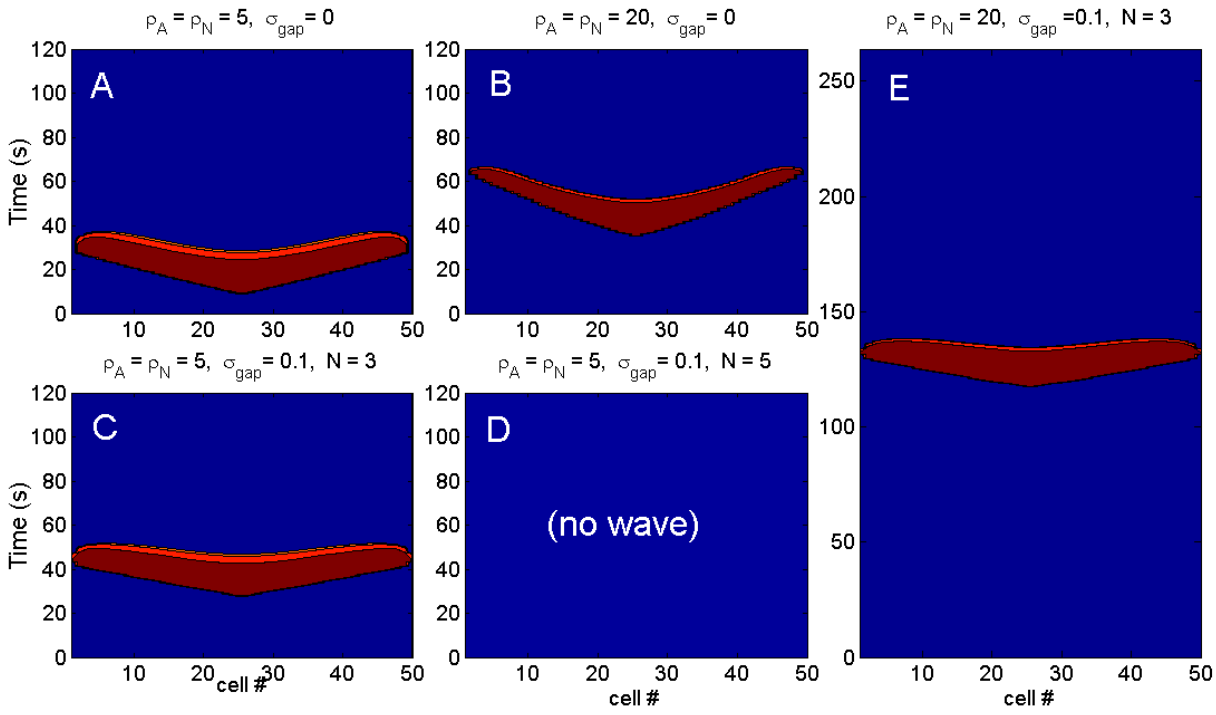

Figure 2: Solutions of the model with simulated $[K^+]_e$ injection at a rate of 5 mM/s until a wave is initiated. 50 neuron-astrocyte pairs are simulated, with the middle four cells stimulated with K^+. Pictured is V_N, with color banding corresponding to potentials greater than -30 mV. Different panels correspond to different values of: i) the pump strenghts, ρ_N and ρ_A; ii) the strength of gap junction connections, σ_{gap}; and iii) the number of neighbors on each side that each astrocyte has gap junction connections with, N. Increasing any of these parameters lengthens the time until a wave is initiated. If these parameters are sufficiently large, then a wave will not be initiated as is the case of panel D.

then there is a significant delay until a wave is initiated. Increasing σ_{gap} or the number of connections can prevent the wave entirely. This is the case in Figure 2D where $\rho_N = \rho_A = 5$, $\sigma_{gap} = 0.1$ and $N = 5$.

To compute the wave speed, we note that the K^+ and Na^+ diffusion coefficients in the extracellular fluid are given by $\overline{D}_K = 1.96 \times 10^{-5}$ cm^2/s and $\overline{D}_{Na} = 1.33 \times 10^{-5}$ cm^2/s [28]. The coefficients D_K and D_{Na}, defined in the Methods section, are obtained from $\overline{D}_K$ and $\overline{D}_{Na}$, scaled by the square of the average distance δ between neurons. In our model, $D_K = .002$ ms^{-1}, $D_{Na} = .00133$ ms^{-1} and $\delta \approx .0313 \times 10^{-2}$ mm. The waves pictured in Figure 2 travel approximately 1-2 cells per second, from which it follows that the wave speed is approximately 2-4 mm/min, consistent with published results [4].

The propagation of the wave is due primarily to the diffusion of K^+ in the extracellular space. That is, elevated extracellular K^+ leads to an increase in a neuron's K^+ Nernst potential. The resulting depolarization increases Na^+ currents, which leads to the upstroke of the neuron's membrane potential. The neuron's K^+ channels then activate, K^+ is released into the extracellular space and then diffuse to the extracellular space of nearby neurons. This may lead to a wave of spreading depolarization. This mechanism was originally proposed by Grafstein [38]. Once a neuron depolarizes, its K^+ and Na^+ ion concentrations slowly recover. As shown in Figure 3, once these concentrations recover sufficiently, the neuron can no longer maintain its depolarized state and returns to physiological resting levels.

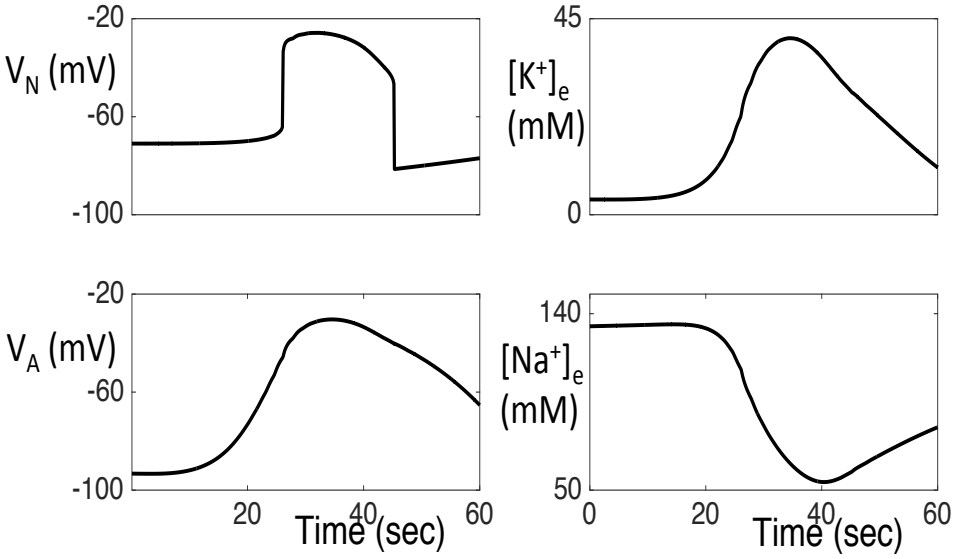

Figure 3: Time evolution of dependent variables V_N, V_A, $[K^+]_e$ and $[Na^+]_e$ corresponding to a fixed neuron/astrocyte pair during a wave of spreading depolarization. Here, $\rho_N = \rho_A = 10$ and $\sigma_{gap} = 0$.

Dependence on parameters. We varied the pump strengths ρ_N and ρ_A independently and quantified the speed and duration of waves, as well as the delay before wave initiation. Results are shown in Figure 4. We find that wave speed decreases with ρ_N and ρ_A, and latency increases, as expected. The duration of depolarization remains relatively constant in ρ_A, but decreases with ρ_N (Figure 4D). The duration varies from roughly 20 seconds, for large neuron pump strengths, to over a minute for small neuron pump strengths. This is consistent with experimental findings and previous models for spreading depression and spreading depolarizations [4, 30]. Figure 4A shows the number of neurons, which depolarize after a wave is initiated. This figure demonstrates that the wave may fail to propagate to the end of the one-dimensional array if the pump strengths are sufficiently large.

With gap junctions, the wave may fail to propagate except for small values of the pump strengths. We demonstrate this in Figure 5, where $N = 5$ and $\sigma_{gap} = 1$. In this case, a wave does not initiate if both ρ_N and ρ_A are greater than 3 μA/cm^2. As before, the latency increases and the speed of propagation decreases with pump strengths. Furthermore, duration of depolarization remains relatively constant in ρ_A, but decreases with ρ_N.

We studied the existence, speed, latency, and duration of depolarization as we varied the gap strength σ_{gap} and the number of neighbors each astrocyte shares a gap junction connection with (Figure 6). If both σ_{gap} and the number of neighbors are sufficiently large, a wave is not initiated. Note that the wave speed and latency are both increasing functions of both σ_{gap} and the number of connections. This suggests that while strengthening gap junction coupling either delays or even prevents a wave, once a wave is initiated, gap junctions promote a greater wave speed.

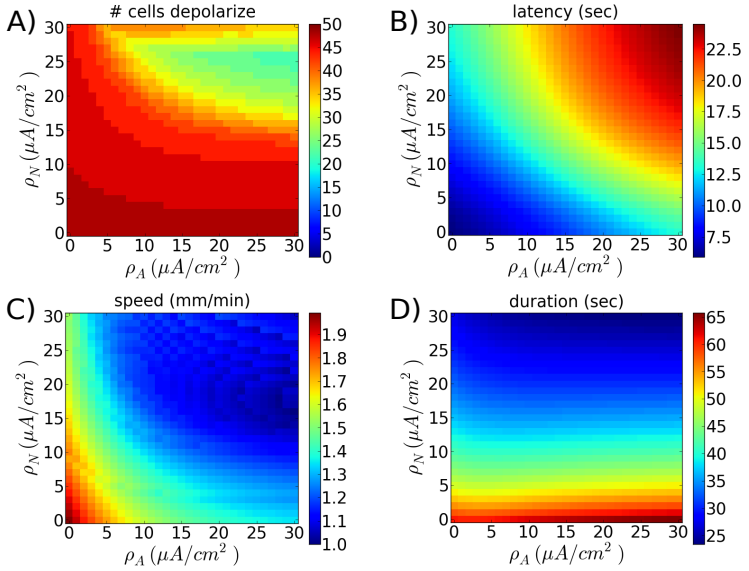

Figure 4: Dependence of wave properties on pump strengths without gap junctions. Shown, as a function of ρ_N and ρ_A, are: (A) the number of cells whose voltage exceeds -40mV, (B) latency (time until one of the neuron's membrane potential reaches -40 mV), (C) wave speed and (D) duration of depolarization at cell V_{24}. Here $\sigma_{gap} = 0$ and K^+ is injected at a rate of 5 mM/sec.

The role of gap junctions in buffering extracellular K^+. We now address the role played by gap junctions in buffering extracellular K^+, thereby delaying or even preventing the initiation of spreading depolarizations. We begin by noting that membrane K^+ currents are typically outward; that is, K^+ ions leave a cell through K^+ channels. So why should elevated K^+ enter the astrocytes and what role do gap junctions play in this?

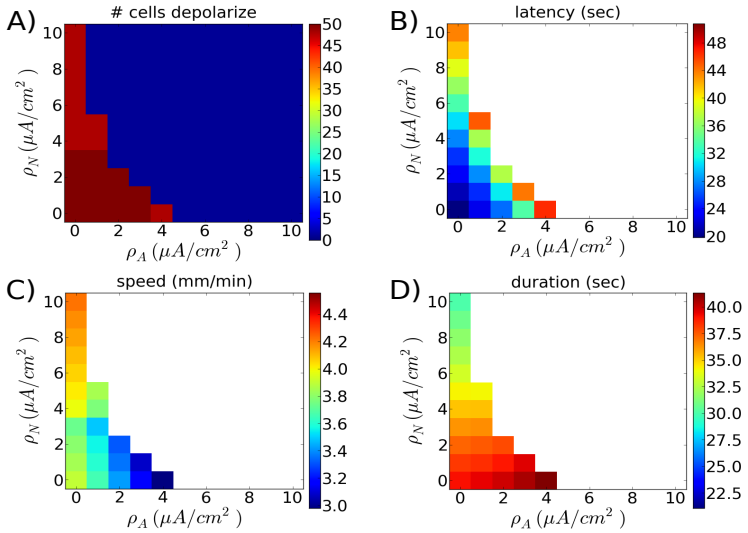

Figure 5: Dependence of wave properties on pump strengths with gap junctions. Shown, as a function of ρ_N and ρ_A, are: (A) the number of cells whose voltage exceeds -40mV, (B) latency (time until one of the neuron's membrane potential reaches -40 mV), (C) wave speed, and (D) duration of depolarization at cell V_{24}. Here $\sigma_{gap} = 1, N = 5$ and K^+ is injected at a rate of 5 mM/sec.

Consider the equation for a K^+ current written using the conductance-based Hodgkin-Huxley formalism: $I_{K,A} = \bar{g}_K(V_A - E_{K,A})$, where $\bar{g}$ is the total conductance. The current is outward if $V_A > E_{K,A}$ and inward if $V_A < E_{K,A}$. As we shall see, the role of gap junctions is to keep $V_A < E_{K,A}$ when there is elevated $[K^+]_e$. This allows astrocytes to sequester extracellular K^+ through K^+ channels.

Consider a fixed astrocyte that is coupled through gap junctions with N other astrocytes as part of a syncytium. Moreover, suppose that there is a sudden increase in $[K^+]_e$ to just the fixed astrocyte. Since $E_{K,A} = \frac{RT}{F} \ln\left(\frac{[K^+]_e}{[K^+]_{i,A}}\right)$, it is clear that an increase in $[K^+]_e$ is accompanied with a corresponding increase in $E_{K,A}$. In isolation, the astrocyte will quickly readjust its intracellular ion concentrations to bring its membrane potential above the new $E_{K,A}$.

An important function of the astrocyte syncytium is maintaining *isopotentiality*. As demonstrated in [35], if N is sufficiently large and the gap junction coupling is sufficiently strong, then the membrane potential of the fixed astrocyte will remain close to that of its coupled neighbors, even when there is a sharp increase in $[K^+]_e$. In other words, a local increase in $[K^+]_e$ to a single astrocyte leads to an increase in that cell's $E_{K,A}$, but not its membrane potential. We may therefore have $V_A < E_{K,A}$ for an extended period, causing K^+ ions to flow into cell through membrane K^+ channels.

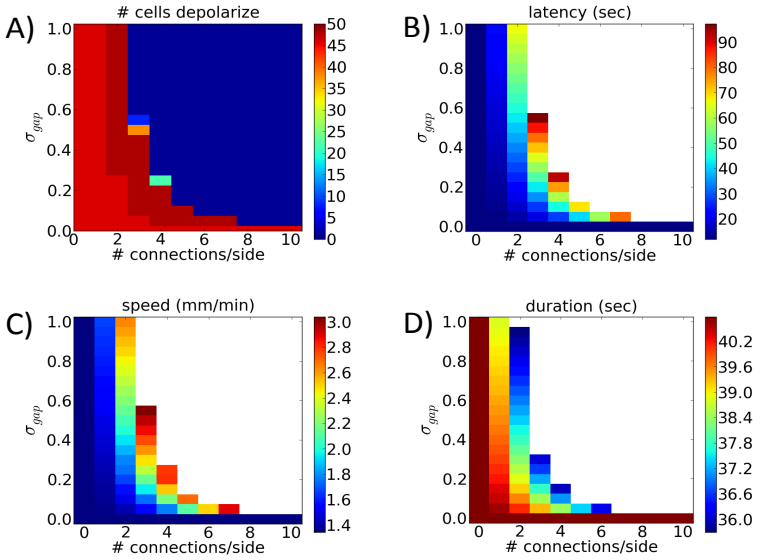

Figure 6: Dependence of wave properties on gap junction coupling strength. Shown, as a function of σ_{gap} and number of neighbors with gap junction connections, are: (A) the number of cells whose voltage exceeds -40mV, (B) latency (time until one of the neuron's membrane potential reaches -40 mV), (C) wave speed, and (D) duration of depolarization at cell V_{24}. Here $\rho_N = \rho_A = 10$ and K^+ is injected at a rate of 5 mM/sec.

To illustrate this computationally, we consider networks of 50 neuron/astrocyte pairs with different degrees of gap junction coupling. Each network begins initially at rest, except we raise the extracellular K^+ concentration of the middle cells, $\mathcal{M} = \{24, 25, 26, 27\}$, to 15 mM. The elevated K^+ can then spread through the network either by diffusion in the extracellular space, uptake into neurons and astrocytes through K^+ channels and ATP pumps, or via gap junctions. These, in turn, lead to changes in both the neuron and astrocyte membrane potentials.

The spatial profile of V_A, $[K^+]_e$ and the K^+ Nernst potentials, $E_{K,N}$ and $E_{K,A}$, at $t = 1$ second are shown in Figure 7. Here we consider a network with no gap junctions ($\sigma_{gap} = 0$) and two networks with gap junctions ($\sigma_{gap} = .3$), with $N = 2$ and 5.

Without gap junctions, V_A always remains above $E_{K,A}$ (Figure 7A). In this case, the K^+ current, $I_{K,A}$, is always outward and decreases in $[K^+]_e$ are due to diffusion of K^+ in the extracellular space and the uptake of K^+ through the ATP pumps. Note that V_A tracks E_K closely and remains depolarized at those cells in which $[K^+]_e$ is elevated.

With gap junctions, there is less of a gradient in V_A (Figures 7B and C). When $N = 5$, V_A is nearly constant. This causes $V_A < E_{K,A}$ at those cells at which K_E is elevated. The K^+ current is now inward and this provides a powerful mechanism for the uptake of elevated extracellular K^+.

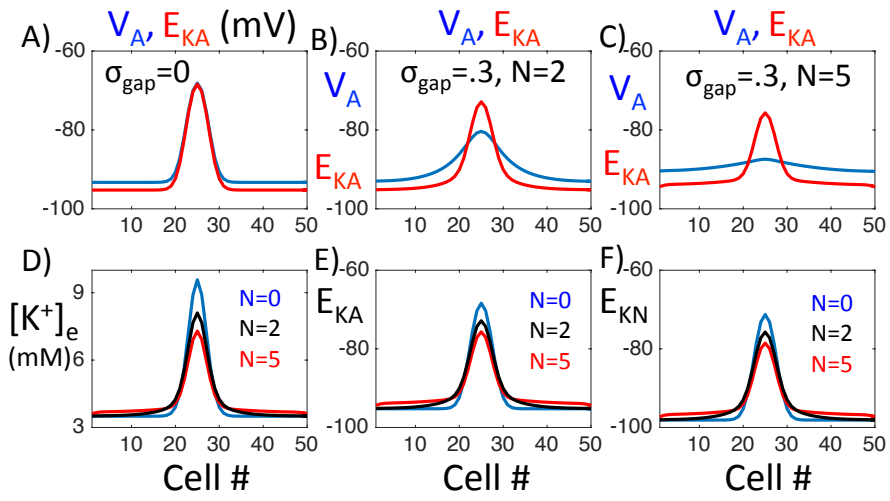

Figure 7: Response to a local increase in extracellular K^+. The network is initially at rest, except we raise the extracellular K^+ concentration of the middle cells to 15 mM. Each panel shows a solution at time $t = 1$ second. (A) Without gap junction coupling: V_A follows $E_{K,A}$. (B) With gap junctions, there is a smaller gradient in V_A. (C) If gap junction coupling is sufficiently large, then V_A is nearly constant. (D) Dependence of $[K^+]_e$ on N, the degree of gap junction coupling. As N increases, cells near the initial disturbance have lower values of $[K^+]_e$, while cells away from the initial disturbance have elevated levels of $[K^+]_e$. (E) and (F) Dependence of the Nernst potentials $E_{K,A}$ and $E_{Na,A}$ on N. As N increases, both astrocytes and neurons near the initial disturbance become less excitable, while cells away from the initial disturbance become more excitable.

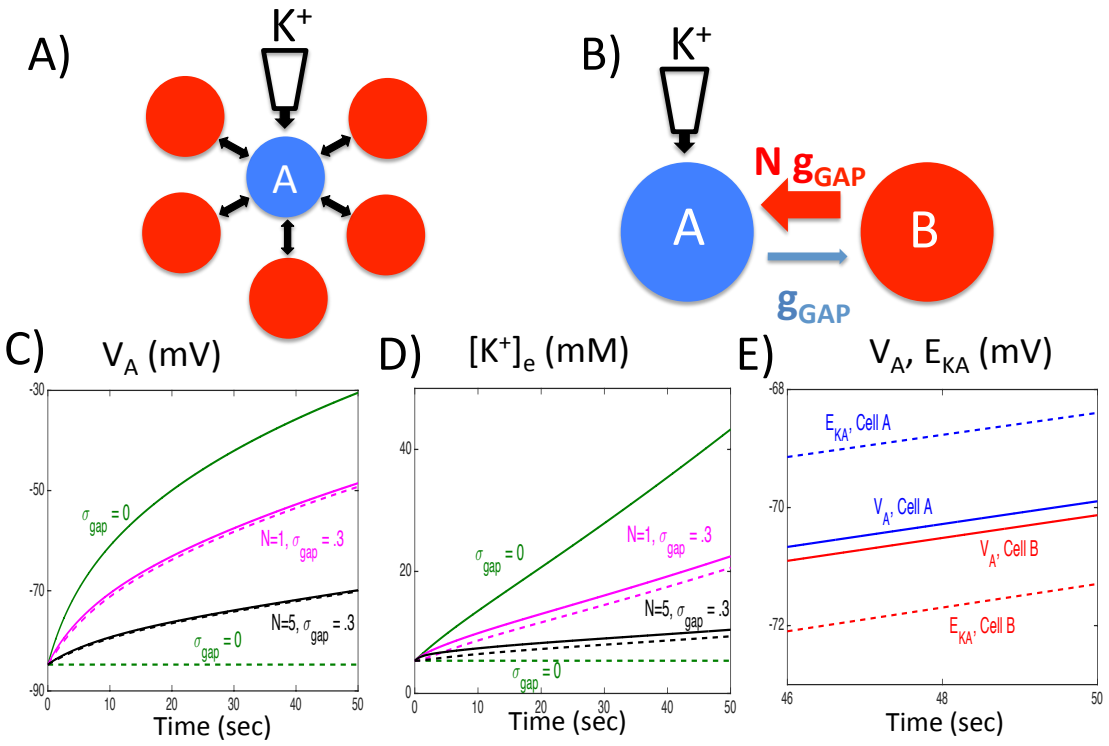

Figure 8: Response of an astrocyte network to a constant increase in $[K^+]_e$. (A) The network consists of $N+1$ astrocytes. Extracellular K^+ is slowly injected into astrocyte $\mathcal{A}$ (blue cell), which is electrically coupled with each of the other N astrocytes (red cells). (B) A two-cell astrocyte model that is equivalent to the network shown in (A). (C) Time evolution of V_A for the two astrocytes, depending on N. Solid curves correspond to astrocyte $\mathcal{A}$ and dashed curves correspond to the other equivalent astrocyte. (D) Time evolution of $[K^+]_e$ for the two astrocytes, depending on N. (E) The membrane potentials and K^+ Nernst potentials of the two cells for $N = 5$ and $\sigma_{gap} = .3$. For each panel, $\rho_A = 10$ and K^+ is injected at a rate of 1 mM/sec.

While gap junctions lead to a lowering of V_A for those cells near $\mathcal{M}$, where K_E is initially elevated, they also result in an increase in V_A for those cells further away from $\mathcal{M}$. This depolarization strengthens $I_{K,A}$, which is outward at these cells, resulting in an increase in $[K^+]_e$, as shown in Figure 7D. With gap junctions, the decrease in $[K^+]_e$ for cells near $\mathcal{M}$ results in a lowering of both the neuron and astrocyte K^+ Nernst potentials, $E_{K,N}$ and $E_{K,A}$. Moreover, the increase in $[K^+]_e$ for cells away from $\mathcal{M}$ results in an increase in both $E_{K,N}$ and $E_{K,A}$. Hence, with gap junctions, neurons and astrocytes near $\mathcal{M}$ are less excitable, while cells away from $\mathcal{M}$ are more excitable. For this reason, it is more difficult to initiate a wave near $\mathcal{M}$, but once a wave is initiated, it propagates with increased velocity.

Next consider a network of just astrocytes, as pictured in Figure 8A. Here there is one astrocyte, which we denote as $\mathcal{A}$, that has gap junction coupling with N other cells. There is no diffusion of ions in the extracellular space. The network is started at rest and we slowly increase $[K^+]_e$ for $\mathcal{A}$ at a fixed rate. We then consider how changes in $[K^+]_e$ and V_A depend on N.

Except for $\mathcal{A}$, the astrocytes are all homogeneous. Therefore, we can lump these other astrocytes together to form a single cell, which we denote as $\mathcal{B}$. Thus the network in Figure 8A is equivalent to the 2-astrocyte network pictured in Figure 8B. If the maximal conductance of the gap junction from $\mathcal{A}$ to $\mathcal{B}$ is g_{gap}, then the maximal conductance of the gap junction from $\mathcal{B}$ to $\mathcal{A}$ is $N \cdot g_{gap}$.

Figures 8C and D show how the time evolution of the membrane potentials and extracellular K^+ concentrations of the two cells depend on N. Each of these decreases as N increases. In particular, the very slow rise in $[K^+]_e$ when $N = 5$ demonstrates there must be a very long delay until $[K^+]_e$ is able to reach a threshold value, needed to trigger a wave of spreading depolarization in the neuron/astrocyte network. Figure 8E shows the membrane potentials and K^+ Nernst potentials for the two cells when $N = 5$. We note that except for $N = 0$, V_A lies below $E_{K,A}$ for cell $\mathcal{A}$, while the opposite is true for cell $\mathcal{B}$.

Discussion

This paper has considered several important issues that have not been discussed in previous modeling studies of cortical spreading depression and spreading depolarizations. Namely, nearly all previous models assumed that the role of the astrocytes is to simply buffer extracellular K^+; this was modeled by including a simple buffering term in the equation for extracellular K^+. Here, we incorporated a detailed biophysical model for the astrocytes. This allowed us to explore more fully the role of specific astrocyte processes in either promoting or preventing wave propagation. Furthermore, earlier modeling papers were primarily concerned in demonstrating that the models were capable of generating spreading depressions for some fixed value of the pump strengths. Here, we identify neuroprotective processes, which may help to prevent or block wave propagation.

Our model is minimal in the sense that it includes only those processes needed to generate the dynamics under study. As noted in [30], the neuron's ability to generate pathological SD behavior does not necessarily depend on abnormal activity of ion channels, but rather a positive feedback based on ion currents causing ion concentration changes. To generate SD, the neuron model includes: i) a voltage dependent Na^+ current that induces a depolarization and then release of K^+ ions into the extracellular space; ii) a slowly inactivating Na^+ current that maintains prolonged excitability, and iii) a fixed leak to stabilize the neuron's resting potential.

The astrocyte model is based on experimental results in [35]. Due to their high and selective membrane permeability to K^+ ions, astrocytes act as nearly perfect potassium electrodes. The astrocyte model, therefore, includes a Kir4.1 type K^+ current and a small Na^+ leak current. The primary role of the astrocytes in this study is to sequester elevated levels of extracellular K^+, thereby preventing the initiation of spreading depolarizations. As shown here and in [35], this requires that each astrocyte belongs to a syncytium consisting of a sufficiently large number of cells with sufficiently strong electrical coupling between cells.

The basic mechanism for extracellular K^+ clearance described here extends the concept of *K^+ spatial buffering*, which was introduced over a half century ago [44]. There have been several experimental, modeling and analytic studies of K^+ spatial buffering since then [40–43]. The basic mechanism for K^+ spatial buffering is the following (see, for example, [39]): A local increase in $[K^+]_e$ produces an astrocyte depolarization that spreads passively to coupled astrocytes. The difference between V_A and $E_{K,A}$ drives K^+ inward at the region where it is raised and outward at distant regions. The result is a net flux of K^+ away from the region where it has accumulated. What we have described in this paper is certainly closely related to this classic description. However, the classic description does not take into account *isopotentiality* of the astrocyte syncytium. With sufficiently strong and wide-spread gap junction coupling, astrocytes near the region of elevated K^+ concentration do not depolarize significantly and this provides a powerful driving force, $E_{K,A} - V_A$, for K^+ uptake through membrane K^+ channels.

Earlier mathematical models and analysis of K^+ spatial buffering also do not take into account isopotentiality. These papers assume the astrocyte membrane potential is passive, in the sense that they ignore the fast time-scales associated with the membrane capacitance. This time-scale is on the order of milliseconds, while earlier models and analysis consider time-scales on the order of tens of seconds. Isopotentiality is achieved on the fast time scale and is critically important to account for the rapid uptake of extracellular K^+ ions, needed to prevent the initiation of the pathological signals.

We previously demonstrated that isopotentiality depends on the number of astrocytes each astrocyte has gap junction connections with [35]. These simulations predict that a syncytium consisting of cells coupled with $\sim$11 neighbors is sufficient to maintain a physiological membrane potential in the presence of a 20 mM extracellular increase in K^+ concentration. Here we demonstrate that, except for very low gap junction coupling strengths, waves of

spreading depolarization will not be generated if N is larger than 5. See Figure 6. This corresponds to each astrocyte being connected to 10 neighboring astrocytes These results are consistent with experimental findings that demonstrate that each hippocampal astrocyte is coupled directly with, on average, 11 of its nearest neighbors [45]

The neuroprotective role of syncytial coupling during diseased states has been under considerable debate. For reviews, see [33, 34]. Naus and co-workers demonstrated that reduced expression of the connexin 43 (Cx43), the most common form of gap junctions, in astrocytes significantly increased the size of ischemic infarcts and they suggested that gap junctional coupling played a critical role in the removal of ions [46, 47]. Farahani et al. proposed a number of possible mechanisms by which gap junction communication may be beneficial following injury [49]. For example, gap junctions may allow for the buffering of toxic metabolites, such as calcium and glutamate, from damaged cells. On the other hand, some studies indicate that gap junction communication may amplify ischemic damage by providing a conduit for the propagation of pro-apoptotic signals between dying and viable astrocytes [48].

As reviewed in [33], the response of Cx43 varies with the severity of injury. Mild to moderate injury appears to lead to increased Cx43 immunoreactivity in the lesion site, while sever injury seems to result in decreased Cx43 immunoreactivity.

Here, we demonstrated with a computational model that gap junction coupling may play a neuroprotective role by preventing the initiation of propagating pathological signals. However, gap junctions may also play a role in amplifying these signals, once they are initiated. These computational modeling results are consistent with those described in [33], who suggest that permanent blockade of Cx43 may not be neuroprotective, but the transient blockade of targeting the window of initial Cx43 upregulation observed following injury is potentially therapeutic.

We have clearly not included many details and processes believed to be important in spreading depolarizations. We have, for example, ignored cell swelling, assumed a simple neuron/astrocyte geometry and the extracellular space is isopotential. Each of these assumptions needs to be reconsidered. The extracellular space may become severely restricted, especially during ischemic-induced cell swelling, in which case extracellular potential gradients may be comparable with intracellular potential gradients. Extending the model from one to two dimensional arrays will allow us to consider more realistic spatial arrangements of the cells, as well as connectivity patterns between cells, and the impact of complex astrocytic branching processes. In future studies, it will be important to explore the roles of such things as changes in cell volume, vasculature, extracellular signals including glutamate, Ca^{2+} dependent processes [16], more realistic geometries, etc. Our hope is that the model considered here will serve as a useful starting point and framework for these further studies.

Conclusion

A syncytium of electrically coupled astrocytes can maintain a physiological membrane potential in the presence of an elevated extracellular K^+ concentration and efficiently distribute the excess K^+ across the syncytium. This provides an effective neuroprotective mechanism for delaying or preventing the initiation of spreading depolarizations. However, gap junctions may also play a role in amplifying these signals, once they are initiated.

Author Contributions

G.H., L.M.M., R.B. and D.T. designed research and performed model development. All authors performed numerical simulations. G.H., L.M.M. and D.T. performed theoretical analysis. G.H., R.B. and D.T. wrote the manuscript. All authors discussed results and commented on the manuscript.

Acknowledgments

This work was partially supported by the US National Science Foundation DMS Awards 1410935 (DT) and 0931642 (Mathematical Biosciences Institute), and the Catalan Grant 2014SGR504 (GH). GH wants to thank the hospitality of the Mathematical Biosciences Institute, while enjoying an Early Career Award, where part of this work was carried out.

References

[1] Dreier JP (2011) The role of spreading depression, spreading depolarization and spreading ischemia in neurological disease. Nat Med 17: 439–447.

[2] Leo AAP (1944) Spreading depression of activity in the cerebral cortex. Journal of Physiology 7: 359–390.

[3] Nedergaard M (1996) Spreading depression as a contributor to ischemic brain damage. Advances in Neurology 71: 75—83.

[4] Pietrobon D, Moskowitz M (2014) Chaos and commotion in the wake of cortical spreading depression and spreading depolarizations. Nature Reviews Neuroscience 15: 379–93.

[5] Risher WC, Ard D, Yuan J, Kirov SA (2010) Recurrent spontaneous spreading depolarizations facilitate acute dendritic injury in the ischemic penumbra. The Journal of neuroscience : the official journal of the Society for Neuroscience 30: 9859–9868.

[6] Somjen GG (2001) Mechanisms of spreading depression and hypoxic spreading depression-like depolarization. Physiological Reviews 81: 1065–1096.

[7] Dirnagl U, Iadecola C, Moskowitz MA (1999). Pathobiology of ischaemic stroke: An integrated view. doi:10.1016/S0166-2236(99)01401-0.

[8] Lauritzen M, Dreier JP, Fabricius M, Hartings JA, Graf R, et al. (2011) Clinical relevance of cortical spreading depression in neurological disorders: migraine, malignant stroke, subarachnoid and intracranial hemorrhage, and traumatic brain injury. Journal of Cerebral Blood Flow and Metabolism 31: 17–35.

[9] Strong AJ, Dardis R (2005) Depolarisation phenomena in traumatic and ischaemic brain injury. Advances and Technical Standards in Neurosurgery 30: 3–49.

[10] Allaman I, Bélanger M, Magistretti PJ (2011) Astrocyte–neuron metabolic relationships: for better and for worse. Trends in Neurosciences 34: 76 - 87.

[11] Haydon PG (2001) GLIA: listening and talking to the synapse. Nature Reviews Neuroscience 2: 185–193.

[12] Nedergaard M (1994) Direct signaling from astrocytes to neurons in cultures of mammalian brain cells. Science 263: 1768-71.

[13] Nedergaard M, Dirnagl U (2005). Role of glial cells in cerebral ischemia. doi: 10.1002/glia.20205.

[14] Zhao Y, Rempe DA (2010) Targeting Astrocytes for Stroke Therapy. Neurotherapeutics 7: 439–451.

[15] Barres BA (2008). The Mystery and Magic of Glia: A Perspective on Their Roles in Health and Disease. doi:10.1016/j.neuron.2008.10.013.

[16] Wang F, Smith N, Xu Q, Fujita T, Baba A, et al. (2012) Astrocytes modulate neural network activity by Ca^{2+}-dependent uptake of extracellular K^{+}. Science Signaling 5: ra26–ra26.

[17] Barreto E, Cressman JR (2011) Ion concentration dynamics as a mechanism for neuronal bursting. Journal of Biological Physics 37: 361–373.

[18] Bennett MR, Farnell L, Gibson WG (2008) A quantitative model of cortical spreading depression due to purinergic and gap-junction transmission in astrocyte networks. Biophysical Journal 95: 5648–5660.

[19] Chang JC, Brennan KC, He D, Huang H, Miura RM, et al. (2013) A mathematical model of the metabolic and perfusion effects on cortical spreading depression. PLoS ONE 8: e70469.

[20] Fröhlich F (2006) Coexistence of tonic firing and bursting in cortical neurons. Physical Review E 74.

[21] Hübel N, Schöll E, Dahlem MA (2014) Bistable Dynamics Underlying Excitability of Ion Homeostasis in Neuron Models. PLoS Computational Biology 10.

[22] Kager H, Wadman WJ, Somjen GG (2002) Conditions for the triggering of spreading depression studied with computer simulations. Journal of Neurophysiology 88: 2700–2712.

[23] Li YX, Rinzel J (1994) Equations for InsP3 receptor-mediated [Ca2+]i oscillations derived from a detailed kinetic model: a Hodgkin-Huxley like formalism. Journal of Theoretical Biology 166: 461–473.

[24] Shapiro BE (2001) Osmotic forces and gap junctions in spreading depression: A computational model. Journal of Computational Neuroscience 10: 99–120.

[25] Somjen GG, Kager H, Wadman WJ (2008) Computer simulations of neuron-glia interactions mediated by ion flux. Journal of Computational Neuroscience 25: 349–365.

[26] Tuckwell HC, Miura RM (1978) A mathematical model for spreading cortical depression. Biophysical Journal 23: 257–276.

[27] Wei Y, Ullah G, Schiff SJ (2014) Unification of neuronal spikes, seizures, and spreading depression. The Journal of Neuroscience 34: 11733-11743.

[28] Yao W, Huang H, Miura R (2011) A continuum neuronal model for the instigation and propagation of cortical spreading depression. Bulletin of Mathematical Biology 73: 2773-2790.

[29] Zandt BJ, ten Haken B, van Dijk JG, van Putten MJAM (2011) Neural dynamics during anoxia and the "wave of death". PLoS ONE 6.

[30] Kager H, Wadman WJ, Somjen GG (2000) Simulated seizures and spreading depression in a neuron model incorporating interstitial space and ion concentrations. Journal of Neurophysiology 84: 495–512.

[31] Kager H, Wadman WJ, Somjen GG (2007) Seizure-like afterdischarges simulated in a model neuron. Journal of Computational Neuroscience 22: 105–128.

[32] Diekman CO, Fall CP, Lechleiter JD, Terman D (2013) Modeling the neuroprotective role of enhanced astrocyte mitochondrial metabolism during stroke. Biophysical Journal 104: 1752–1763.

[33] Chew SSL, Johnson CJ, Green CR, Danesh-Meyer HV (2010) Role of connexin43 in central nervous system injury. Experimental Neurology 225: 250-261.

[34] Chen Y, Swanson RA (2003) Astrocytes and brain injury. Journal of Cerebral Blood Flow & Metabolism 23: 137-149.

[35] Ma B, Bucklew R, Du Y, Kiyoshi CM, Alford CC, Wang W, McTigue, Enyeart JJ, Terman D, Zhou M (2016) Gap junction coupling confers isopotentiality on astrocyte syncytium. Glia 63: 214-226.

[36] Ermentrout GB, Terman DH (2010) Mathematical foundations of neuroscience, volume 35 of *Interdisciplinary Applied Mathematics*. Springer, New York, xvi+422 pp.

[37] Ermentrout GB (2002) Simulating, analyzing and animating dynamical system: a guide to XPPAUT for researchers and students. SIAM 14.

[38] Grafstein B (1956) Locus of propagation of spreading cortical depression J Neruphysiology 19: 308-316.

[39] Orkand RK (1986) Glial-interstitial fluid exchange. Ann NY Acad Sci 481: 269-272.

[40] Kofuji P, Newman EA (2004) Potassium buffering in the central nervous system. Neuroscience 129: 1045-1056.

[41] Gardner-Medwin AR, Nicholson C (1983) Changes of extracellular potassium activity induced by electric current through brain tissue in the rat. J Physiol 335:375-392.

[42] Gardner-Medwin AR (1983) Analysis of potassium dynamics in brain tissue. J Physiol 335:393-426.

[43] Chen KC, Nicholson C (2000) Spatial Buffering of Potassium Ions in Brain Extracellular Space. Biophysical Journal 78:2776-2797.

[44] Orkand RK, Nicholls JG, Kuffler SW (1966) Effect of nerve impulses on the membrane potential of glial cells in the central nervous system of Amphibia. J Neurophysioloty 29: 788-806.

[45] Xu G, Wang W, Zhou M (2014) Spatial Organization of NG2 Glial Cells and Astrocytes in Rat Hippocampal CA1 Region. Hippocampus 24: 383-395.

[46] Nakase T, Fushiki S, Sohl G, Theis M, Willecke K, Naus CC (2003) Neuroprotective role of astrocytic gap junctions in ischemic stroke. Cell Commun Adhes 10: 413-417.

[47] Siushansian R, Bechberger JF, Cechetto DF, Hachinski VC, Naus CC (2001) Connexin43 null mutation increases infarct size after stroke. J Comp Neurol 440: 387-394.

[48] Lin JH, Weigel H, Cotrina ML, Liu S, Bueno E, Hansen AJ, Hansen TW, Goldman S, Nedergaard M (1998) Gap-junction-mediated propagation and amplification of cell injury. Nature Neuroscience 1: 494-500.

[49] Farahani, R., Pina-Benabou, M.H., Kyrozis, A., Siddiq, A., Barradas, P.C., Chiu, F.C., Cavalcante, L.A., Lai, J.C., Stanton, P.K., Rozental, R. (2005) Alterations in metabolism and gap junction expression may determine the role of astrocytes as good samaritans or executioners.. Glia 50: 351-361.